

Improving the Flow Cytometry-based Detection of the Cellular Uptake of Gold Nanoparticles

Yue Wu,[†]

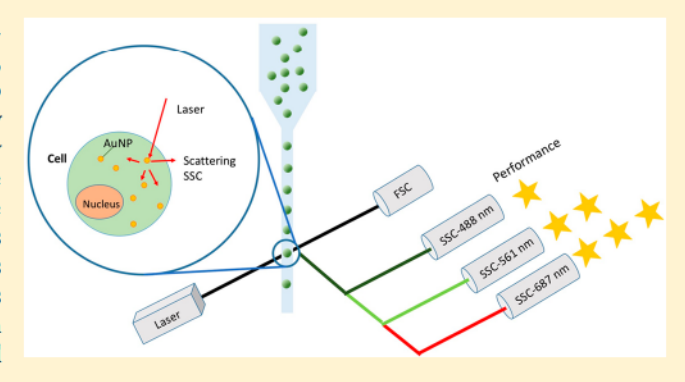
Moustafa R. K. Ali,*,^{†,‡}

Kamaria Dansby,[†] and Mostafa A. El-Sayed*,[†]

Laser Dynamics Lab (LDL), School of Chemistry and Biochemistry, Georgia Institute of Technology, Atlanta, Georgia 30332-0400, United States

Supporting Information

ABSTRACT: Due to the considerable amount of applications of gold nanoparticles (AuNPs) in biological systems, there is a great need for an improved methodology to quantitatively measure the uptake of AuNPs in cells. Flow cytometry has the ability to measure intracellular AuNPs by collecting the light scattering from a large population of live cells through efficient single cell analysis. Traditionally, the side scattering setting of the flow cytometer, which is associated with a 488 nm excitation laser (SSC channel), is used to detect nanoparticle uptake. This method is limited as AuNPs do not have the optimized response when excited with this laser. Here, we reported that the use of more red-shifted excitation lasers will greatly enhance the optical signal needed



for the flow cytometry-based detection of AuNSs (26 nm in diameter) and AuNRs (67 nm × 33 nm, length × width) uptake in triple negative breast cancer cells (MDA-MB-231).

INTRODUCTION

Gold nanoparticles (AuNPs) are key materials that are widely used in diverse scientific fields such as chemistry, biology, medicine, and engineering.1-4 AuNPs have great and unique optical properties. When AuNPs are excited by light at specific wavelengths, the interaction between the electromagnetic field of light and the conduction electrons of AuNPs cause the electrons to oscillate in resonance with the frequency of light,5 which is termed the surface plasmon resonance (SPR). The SPR gives AuNPs unique optical properties, which include their large scattering cross sections, that are 5 orders of magnitude higher (from 80 nm gold nanospheres) than the light emission from fluorescent molecules such as fluorescein.⁶ The strong scattering of AuNPs allow them to be easily detected by scattering-based detection methods. Additionally, AuNPs can be easily surface-modified with many types of functional groups, such as proteins, peptides, and oligonucleotides, while still maintaining their optical properties.

The amount of intracellular AuNPs can be positively correlated to their possible effects at cellular levels. Currently, several methods can be used for measuring intracellular AuNPs. Element analysis techniques such as inductively coupled plasma (ICP)-based spectroscopic methods (including optical emission spectrometry (ICP-OES) and mass spectrometry (ICP-MS)) are commonly regarded as the most accurate AuNP quantification methods. In addition, spectroscopic methods that use UV-vis and Beer-Lambert's law which correlate the AuNP concentration with the absorbance at their SPR peak could also be regarded as a fast detection of average AuNP uptake,9 though the accuracy might not be comparable to the element analysis techniques. However, an obvious drawback of the aforementioned methods is that they only provide the average amount of AuNP intracellular content, with little to no information regarding the distribution within the cell population or spatial location. 10 Many microscopic methods that provide the distribution and spatial location of AuNPs are used in quantifying AuNPs as well. These methods include transmission electron microscopy (TEM) and optical microscopies such as dark-field microscopy (DFM) that is based on light scattering. 10,11 Although TEM provides much higher resolution (Ångstrom to nanometer) when compared to DFM (>250 nm) for measuring intracellular spatial distribution, it requires complex and laborious sample section preparation with limits in the number of cells that can be measured. Flow cytometry (FCM) is a cell sorting method that can detect the fluorescence or scattering from cells. AuNPs uptake can be quantified from the side scattering signal (SSC) as the presence of AuNPs increases the SSC response from the flow cytometer. A recent article measured the SSC signal from intracellular AuNPs and compared this data with similar data from the ICP-MS, which showed a perceptible agreement between the two methods. 12 The FCM method is as beneficial as it is efficient at analyzing intracellular AuNPs without laborintensive and complicated sample preparation. It is very

Received: May 13, 2019 Accepted: October 24, 2019 Published: October 24, 2019



effective as it measures the average amount of AuNP intracellular content and also provides information regarding AuNP distribution within the cell population. In addition, we can sort cells by way of AuNP content using FCM which is useful for further studies, such as proteomics and gene sequencing.

Traditionally, the side scattering mode with 488 nm laser illumination (SSC channel) is used for measuring the intracellular AuNP amount; 12 however, the AuNP scattering detection is not optimized under the 488 illumination laser as it is not close to the SPR peak of the AuNPs. For most of the spherical AuNPs (AuNSs), the SPR peak is around 510-550 nm, while for Au nanorods (AuNRs), the SPR peak will be a higher wavelength ranging from the visible range of the electromagnetic spectrum to the infrared region. In addition, the aggregation of AuNPs inside cells causes a red shift of the SPR peak. 13 Moreover, the scattering from biological tissues decrease when red-shifting the incident light, 14 which makes the scattering from AuNP more sensitive to detect. Therefore, we hypothesized that the use of an incident light with a higher wavelength closer to that of the SPR peak of the intracellular AuNPs is a promising approach to improving the flow cytometry-based detection of intracellular AuNPs by way of SSC signals.

Herein, we measured the FCM side scattering of intracellular AuNSs (26 nm diameter) and AuNRs (33 nm × 67 nm, width ×x length) using incident lasers with different wavelengths. Our results show that by red-shifting the illuminating laser wavelength, the signal will be greatly enhanced for detecting both AuNSs and AuNRs cellular uptake using FCM.

METHODS

Materials. Tetrachloroauric acid trihydrate (HAuCl₄· 3H₂O), trisodium citrate, silver nitrate (AgNO₃), sodium borohydride (NaBH₄), ascorbic acid, cetyltrimethylammonium bromide (CTAB), paraformaldehyde, glutaraldehyde, ethylenediaminetetraacetic acid (EDTA), HEPES, and bovine serum albumin (BSA) were purchased from Sigma (St. Louis, MO). Dulbecco's modified Eagle's medium (DMEM), fetal bovine serum (FBS), antibiotic/antimycotic solution, phosphate-buffered saline (PBS), and 0.25% trypsin/2.2 mM EDTA solution were purchased from VWR. Methoxypolyethylene glycol thiol (mPEG-SH, MW 5000) was purchased from Laysan Bio, Inc. Cell-penetrating peptide RGD (RGDRGDRGDPGC) and nuclear localization sequence NLS (CGGGPKKKRKVGG) peptides were purchased from GenScript, Inc. (Piscataway, NJ). All the water used in the experiments was purified with a Milli-Q system from Millipore (Milford, MA).

Instrumentation. Gold nanoparticles were imaged under a JEOL 100CX-2 transmission electron microscope (TEM). The average sizes of AuNPs were measured by ImageJ software based on the TEM images. The spectra of AuNPs were obtained using an Ocean Optics HR4000CG ultraviolet—visible-near—infrared (UV—Vis—NIR) spectrometer. Flow cytometry experiments were performed on BD LSR Fortessa supplied with 488, 561, and 687 nm excitation lasers. The BioTek Synergy H4 hybrid plate reader was used for reading the XTT cell viability assay results. Dark-field microscopy is equipped with Lumenera Infinity2 CCD camera.

Gold Nanoparticle Synthesis, Conjugation, Characterization. Gold nanospheres (AuNSs) with an average

diameter of 26 nm were synthesized using the citrate reduction method. Here, 500 mL of 0.254 mM HAuCl $_4$ ·3H $_2$ O solution was heated until boiling and reduced by adding 9 mL of 0.35% citrate solution quickly to the precursor solution. The solution was left under heat, and an observable color change occurred from light yellow to burgandy upon reaction completion. The solution was then removed from the heating apparatus and cooled with a water bath. Newly synthesized AuNSs were purified via centrifugation with initial conditions being 1500g for 5 min and adding DI H $_2$ O to the pellets.

Gold nanorods were synthesized using a seed growth method developed by our lab. 15 Briefly, to prepare Au seed, CTAB solution (5 mL, 0.20 M) and HAuCl₄ (5.0 mL of 0.00050 M) was mixed with stirring. Then, 0.60 mL of ice-cold NaBH₄ (0.010 M) was added. The mixture was vigorously stirred to generate Au seed for 2 min. A brownish yellow solution was formed. Next, to prepare the growth solution, 5.0 mL of HAuCl₄ (1.0 mM), 270 μ L of AgNO₃ (4.0 mM), 5.0 mL of CTAB (0.2 M), and 70 μ L of ascorbic acid (78.8 mM) were gently mixed. The prepared Au seed (12.0 μ L) was then added to the growth solution and allowed to react with no disturbance for hours. The as-synthesized AuNRs were washed by DI H2O via centrifugation twice with initial conditions being 10,000g for 10 min and 5000g for 10 min. TEM was used for imaging the sizes, and the homogeneity of the AuNPs prepared.

For surface modification, the purified nanoparticles were treated with polyethylene glycol (PEG, 1 mM) as an initial conjugation step and left on a shaker overnight with 1:1,000 (AuNP:PEG). RGD (1 mM) and NLS (1 mM) were added concurrently, with 1:10,000 (AuNP:RGD) and 1:100,000 (AuNP:NLS) after the initial conjugation step and shaken overnight. Conjugated AuNPs were then centrifuged and redispersed in DI water. To test the surface modification, UV–Vis–NIR spectrometer were used. The AuNPs' spectra revealed a red shift due to the changes in the dielectric constant of the surrounding environment of AuNPs, which offers verifiable evidence of conjugation success.

The molar concentrations (C) of the AuNPs (AuNSs and AuNRs) are calculated based on Beer's law $A = \varepsilon \times b \times C$, where A is the extinction of AuNPs (O.D.), ε is the molar extinction (L mol⁻¹ cm⁻¹), and b is the path length of the sample (1 cm). Both of the AuNSs and AuNRs have $\varepsilon \sim 3 \times 10^9 \, \text{L mol}^{-1} \, \text{cm}^{-1}$ according to the literatures, ^{16–18} due to their specific sizes and/or aspect ratios.

Cell Culture and Incubation with AuNPs. Human breast adenocarcinoma MDA-MB-231 cells were cultured in Dulbecco's modified Eagle media (DMEM) (without Phenol red) with 1% antibiotic and 10% fetal bovine serum under standard incubation conditions (5% CO₂, 37 °C). Cells were treated with differing concentrations of AuNSs and AuNRs (C0, control no AuNPs; C1, 0.033 nM; C2, 0.083 nM; C3, 0.17 nM; C4, 0.33 nM; and C5, 0.5 nM) for 24 h. UV-vis-NIR spectra were taken of media solutions with varying concentrations of AuNSs and AuNRs before and after a 24 h incubation period. The differences in the absorbance peaks correspond to a quantification of cellular uptake. The cellular uptakes of AuNPs were also measured by dark-field microscopy. For dark-field imaging, the cells were fixed with paraformaldehyde and glutaraldehyde and subsequently imaged with a Lumenera Infinity2 CCD camera.

Cell Viability Assay. To examine the toxicity effect of the AuNPs, XTT cell viability assays were performed according to

the Biotium experimental protocol, in which the XTT activation reagent was mixed with the XTT solution and added to cells. After a 24 h incubation time with AuNPs, absorbance signals from cells were obtained via a plate reader. Background absorbance was subtracted from signal absorbance to collect normalized absorbance values.

Flow Cytometry Measurements. Following AuNP treatment, cells were trypsinized, centrifuged at 1500g for 5 min, and resuspended with sorting buffer composed of 1% FBS in phosphate buffer saline (PBS), 1 mM EDTA, and 25 mM HEPES. The samples were then washed with PBS three times and fixed with paraformaldehyde. Samples were analyzed using a flow cytometer supplied with 488, 561, and 687 nm excitation lasers. Side scattering signals (SSC) from cell samples were collected from varying excitation laser sources and detected with corresponding detection channels. Data output was analyzed utilizing the FlowJo software. Signals were transformed into histogram plots to visualize the comparisons among detection channels and excitation laser combinations.

Data Analysis. A two-tailed t-test was performed to determine statistical significance. The analyses were performed with the alpha type error set at 0.05. To compare the FCM intensities between different laser groups, the intensities were scaled with the maximum value in each group to be 1. All the values are thus located between [0, 1], enabling comparison between different conditions.

RESULTS

Gold Nanoparticle Preparation, Cellular Uptake, and Cell Viability. AuNSs with an average size of 26.2 ± 4.9 nm and a surface plasmon resonance (SPR) peak of 528 nm were synthesized using the citrate reduction method. AuNRs with an average size of $67.8 (\pm 9.5)$ nm $\times 33.1 (\pm 3.2)$ nm (length \times width) were synthesized using the seed-mediated method. The AuNRs exhibit a dominant longitudinal SPR peak of 650 nm (fwhm = 80 nm) and a small transverse peak at 520 nm (fwhm = 30 nm). The characterization of AuNSs and AuNRs are shown in Figure S1 (TEM and UV-vis-NIR spectra). The AuNRs were washed by DI H_2O twice to remove extra CTAB in preparation for surface modification. Both of these types of nanoparticles have been widely utilized in biological and medical research due to their favorable biocompatibility. 19,20

To generate adequate cellular uptake of AuNPs, both the AuNSs and AuNRs were functioned with methoxy-polyethylene glycol thiol (PEG), Arg-Gly-Asp (RGD) peptides, and nuclear localization signal (NLS, CGGGPKKKRKVGG) peptides. The conjugation of PEG enhances biocompatibility.21 RGD is a peptide bound to surface integrins which are often overexpressed on the surfaces of many types of cancer cells.^{22,23} By conjugating RGD, we are able to selectively target cancer cells. NLS was introduced to increase the cellular uptake of AuNPs and accumulate at the nuclear area of cells. 24,25 The successful conjugations are evident by the UVvis spectra which shows the red-shifting of SPR peaks (for AuNSs: before conjugation, 528 nm; after PEG coating, 531 nm; after RGD/NLS coating, 533 nm; for AuNRs: before conjugation, 650 nm; after PEG coating, 651 nm; after RGD/ NLS coating, 652 nm; Figure S1) due to the change of dielectric constant.

The uptake of the AuNPs were first measured by dark-field (DF) microscopy. The MDA-MB-231 cells were incubated with media (without phenol red) with or without AuNPs (Ctrl, no nanoparticles added; AuNSs and AuNRs conjugated with

PEG; AuNSs and AuNRs conjugated with NLS) for 24 h. The scattering light from AuNPs allows DF imaging to be considered a sensitive method for measuring cellular uptake. As shown in Figure 1, enhanced light scattering was observed

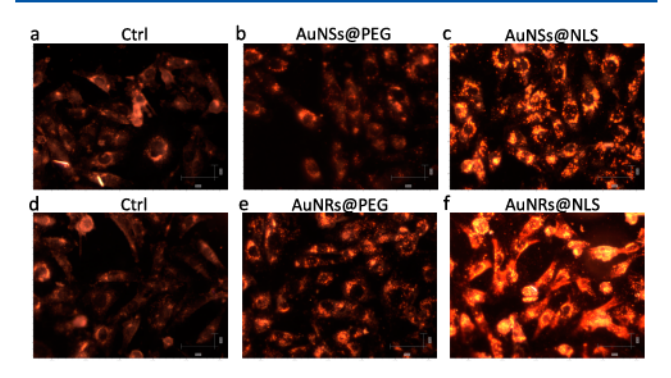


Figure 1. Dark-field images of MDA-MB-231 cells incubated with or without AuNSs (a-c) and AuNRs (d-f). The PEG conjugated gold nanoparticles (AuNSs@PEG and AuNRs@PEG) act as controls for their minor cellular uptake compared with the NLS conjugated ones (AuNSs@NLS and AuNRs@NLS).

for cells incubated with AuNRs@NLS and AuNSs@NLS, compared with Ctrl and with ones conjugated with PEG (which exhibits very minor uptake). The cell viability after AuNPs incubation was measured using an XTT assay (Figure S2). An XTT assay is widely adopted by the community for measuring the AuNP's cytotoxicity, 26-29 and the results show consistency with other methods according to our previous reports. No significant decrease in cell viability was observed after 24 h of AuNP incubation.

Flow Cytometry Method Development for Measuring Cellular Uptake of Gold Nanoparticles. In flow cytometry, there are two modes of scattering measurements: side scattering and forward scattering. The forward scattering channel (FSC) intensities of the MDA-MB-231 cells incubated with AuNPs were similar to those of the controls (Figure S3), which is in agreement with previous reports. 12,31 The side scattering channel (SSC) usually indicates the scattered light collected at the perpendicular direction (90°) of the incident laser (usually 488 nm), which is commonly used as an indication of the cell's internal complexity or granularity. When nanoparticles are internalized into the cells, they increase the complexity of cells which could be attributed to the increased SSC intensity. Several studies have indicated that when cells uptake gold, TiO2, and ZnO nanoparticles, the SSC intensity increases. 12,32,33

Due to the high scattering coefficients of AuNPs (~5 orders of magnitude greater than conventional fluorescent dyes), SSC could be especially beneficial for detecting signals from AuNPs. The SSC supplied with a 488 nm laser illumination is a commonly used setting for flow cytometry-based detection of intracellular AuNPs but is not optimized for detecting AuNPs. For most AuNPs, their SPR peaks locate at a higher wavelength from the visible range to infrared. In addition, the aggregation of AuNPs inside cells will cause a red shift of the SPR peak. Turthermore, the background scattering of cells decrease when the incident light is at higher wavelength, which is promising in improving the flow cytometry detection for AuNPs using the SSC.

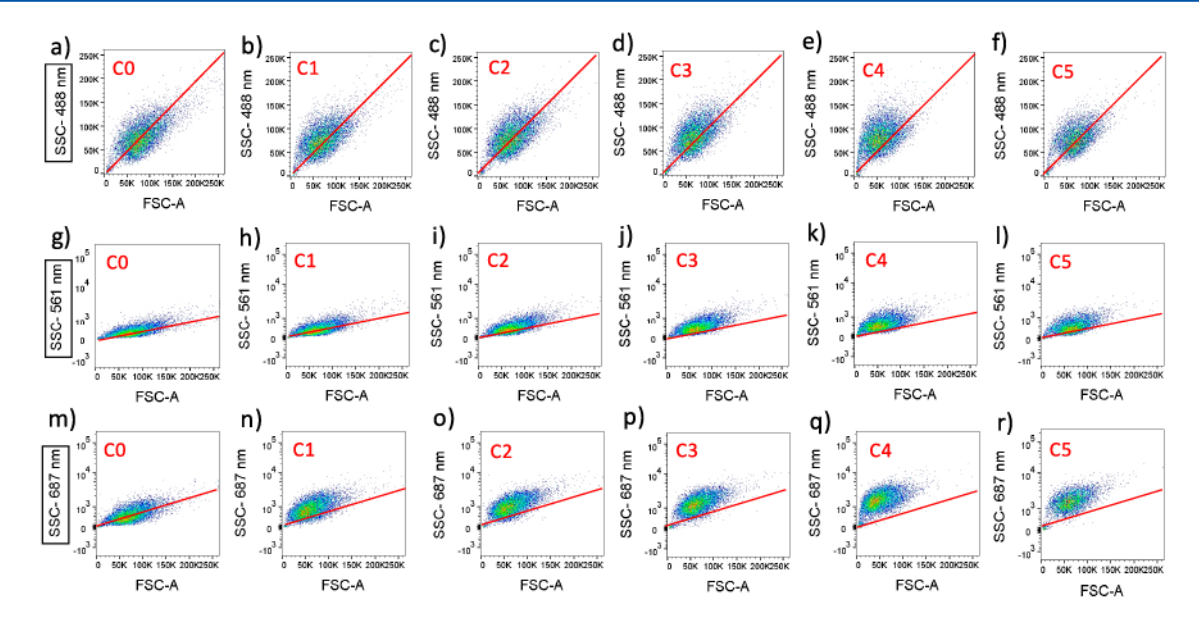


Figure 2. Flow cytometry scatter plots of MDA-MB-231 cells incubated with different concentrations of AuNSs in DMEM media (sample C0, control no AuNPs; C1, 0.033 nM; C2, 0.083 nM; C3, 0.17 nM; C4, 0.33 nM; and C5, 0.5 nM). The plots are side scattering (SSC-A) versus forward scattering (FSC-A) under different incident lights (a-f) 488 nm; (g-l) 561 nm; (m-r) 687 nm). Redlines: reference lines for comparing; same in (a-f), (g-l), and (m-r), respectively).

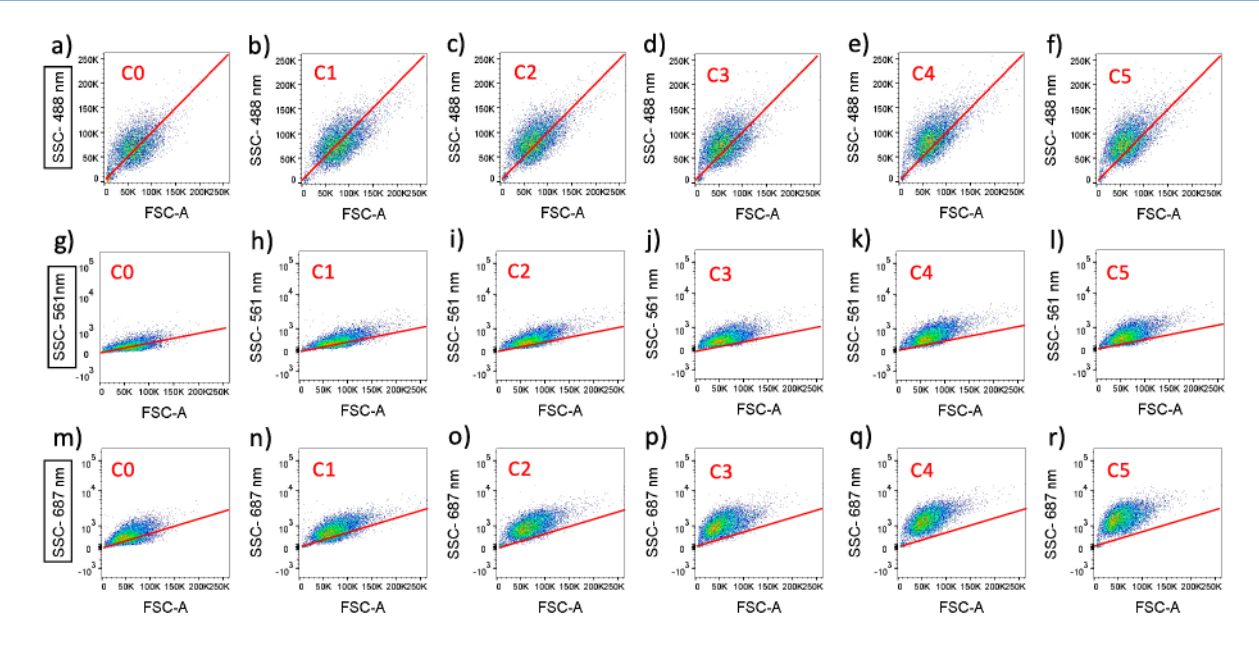


Figure 3. Flow cytometry scatter plots of MDA-MB-231 cells incubated with different concentrations of AuNRs in DMEM media (sample C0, control no AuNPs; C1, 0.033 nM; C2, 0.083 nM; C3, 0.17 nM; C4, 0.33 nM; and C5, 0.5 nM). The plots are side scattering (SSC-A) versus forward scattering (FSC-A) under different incident lights (a-f) 488 nm; (g-l) 561 nm; (m-r) 687 nm). Redlines: reference lines for comparing; same in (a-f), (g-l), and (m-r), respectively).

The conventional 488-SSC was examined first, and the result is shown in Figure S4. The cells incubated with 0.33 nM AuNPs did not show an obvious distinction in the 488-SSC channel when compared with the control. Therefore, to optimize the incident laser, three different incident lasers (488, 561, 687 nm) were used. The scattering intensities were collected for different samples (C0–C5). As shown in Figure 2 (for AuNSs) and Figure 3 (for AuNRs), the SSC intensities increase when the intracellular AuNPs increase. The 687 nm incident laser gives the most significant change when measuring cells with varying intracellular AuNPs concentration

(Figure 2m-r, 3m-r), while 488 nm, which is the default SSC channel laser, gives the worst performance (Figure 2a-f, 3a-f). We can also easily compare the three lasers in the histograms as shown in Figure 4. Therefore, optimizing the incident laser could greatly assist the detection of intracellular plasmonic nanoparticles using flow cytometry.

The quantitative relationship between the scattering intensities and the amount of AuNPs from UV—vis measurements were examined. To compare the performances of the three different incident lasers, the flow cytometry intensities were normalized. The relationship between the flow cytometry

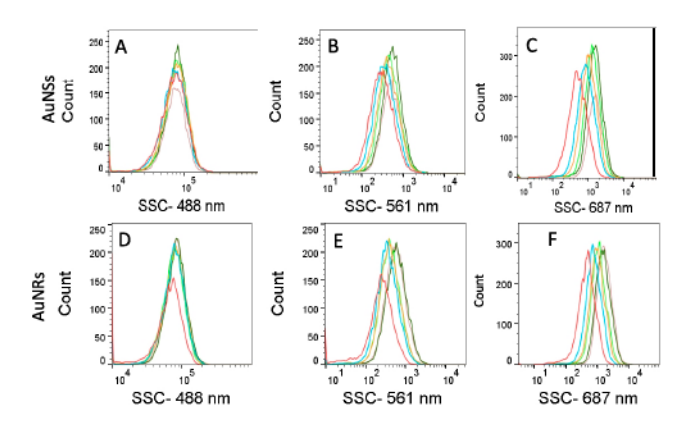


Figure 4. Side scattering intensity (SSC-A) histograms of MDA-MB-231 cells with different incident light wavelengths (488 nm, A for AuNSs and D for AuNRs; 561 nm, B for AuNSs and C for AuNRs; 687 nm, C for AuNSs and F for AuNRs). Cells with different intracellular concentrations were measured. Red, blue, orange, light green, dark green, and tan lines represent samples C0–C5 (C0, Ctrl; C1, 0.033 nM; C2, 0.083 nM; C3, 0.17 nM; C4, 0.33 nM; and C5, 0.5 nM) for 24 h.

and UV-vis data was fitted with a linear function, as shown in Figure 5a and b. The 687 nm incident laser gives the largest

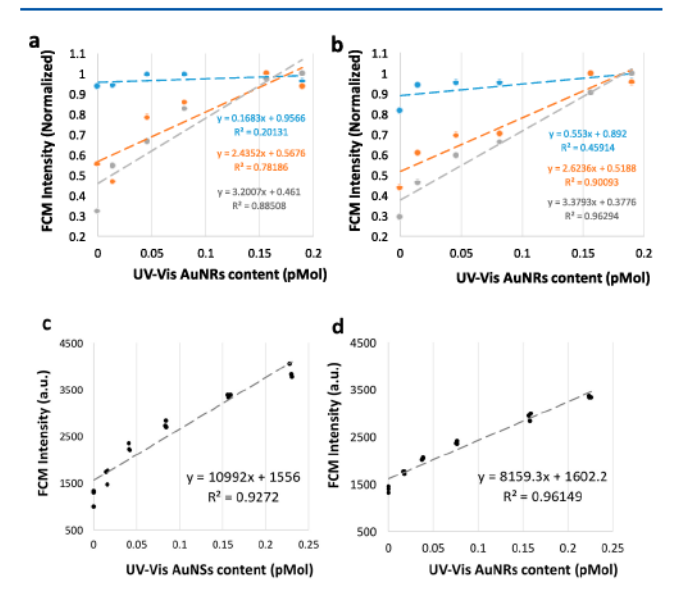


Figure 5. Cellular AuNPs versus FCM side scattering intensities, including linear regression lines: (a) gold nanospheres (AuNSs) and (b) gold nanorods (AuNRs). Blue: 488 nm incident laser; orange: 561 nm incident laser; black: 687 nm incident laser. Reproducibility of the flow cytometry method using 687 nm laser for (c) gold nanospheres (AuNSs) and (d) gold nanorods (AuNRs). Three replications were included. Normalized intensities are used in (a) and (b) for comparing the three incident lasers.

slope of fitting and much improved R² values when compared with the other two lasers. To examine the reproducibility of the flow cytometry method, three replications of 687 nm SCC were conducted, and results are shown in Figure 5c and d, indicating the reproducibility of the FCM method.

DISCUSSION

Gold nanoparticles are widely studied as intracellular imaging probes or as therapeutic reagents. Herein, by improving the sensitivity of the flow cytometry-based detection of intracellular AuNPs, through simply increasing the incident laser wavelength and collecting the scattering signals, we are able to distinctly differentiate single cells with different AuNPs content.

For this method, the limit of detection (LOD) corresponds to around 0.015 pMol AuNPs in each sample (calculation according to reported method³⁴). Despite the large dynamic range of flow cytometry, a practical dynamic range here may only be less than 2 orders of magnitude as it is largely limited by the cells' ability to uptake AuNPs (without causing significant toxicity). Compared with element analysis techniques such as ICP, which are commonly regarded as the most accurate AuNP quantification methods, this method has a higher detection limit and a smaller dynamic range. However, FCM has unique ability which is not obtained by other methods, making it very powerful in certain applications. First, it is efficient at analyzing intracellular AuNPs without laborintensive and complicated sample preparation procedures. Second, the collection of light scattering signals from large populations of live cells through efficient single cell analysis makes it effective for measuring not only the average amount of AuNP intracellular content, but it also provides information regarding AuNP distribution within a cell population. In addition, FCM is not destructive to cells as it is biologically compatible. We can also sort cells based on AuNP content using FCM which is useful for further studies, such as proteomics and gene sequencing.

The objects (which usually are cells or particles with size range of $1-40 \mu m^{33}$) in flow cytometry detection usually require fluorescent labels. However, several types of nanoparticles present high scattering cross sections, which enable sensitive scattering detection for their existence in cells. TiO₂ nanoparticles, for example, are used as ingredients in sunscreen and paint and can absorb UV light. As the default, the flow cytometry side scattering channel (488 nm) is close to the extinction range of TiO2. The resulting resolution has been reported to differentiate cell samples with and without ${\rm TiO_2}$, using the default setting of SSC channel in flow cytometry. 31,32 Zucker and Daniel claimed that by using flow cytometry they were able to detect as low as 5-10 TiO2 nanoparticles per cell, which is very sensitive.³² In addition, Ag nanoparticles, which present a SPR at around 400-500 nm, have strong scattering at this range and are also suitable for the default 488 nm SSC channel.^{35,36} For the internalization of other types of nanoparticles, such as CuO,³⁷ superparamagnetic iron oxide nanoparticles (SPIONs),³⁸ ZnO₂,⁵³ are used, and the use of the default 488 SSC might also be utilized for intracellular detection according to previous reports. 12 However, the scattering signal from AuNPs under 488 nm is not optimized. In our results, we demonstrate this by achieving stronger scattering signals from intracellular AuNPs with the use of more red-shifted incident lasers.

We observed that the 687 nm incident laser as opposed to the 561 nm laser had the best performance for AuNSs even though its SPR is closer to 561 nm. We believe this observation is most likely due to the presence of AuNS aggregates inside cells that red shift the SPR peak, as shown by our previous studies. For instance, we have observed that 30 nm single AuNSs form aggregates inside cells and shift the SPR peak to 641 nm. Moreover, the aggregates could greatly enhance the scattering intensity due to the formation of hot spots, which greatly enhance the sensitivity of detection under 687 nm

incident laser. Concerning the effect of aggregation on the quantification and reproducibility, our results showed that good linearity in regard to AuNP content, as well as good reproducibility, can still be achieved, in agreement with previous observations. 12,38

It is widely recognized that when cells undergo apoptosis, the shrinkage of the cell body will cause a decrease in the FSC signal and an increase of the cell granularity (due to the apoptotic body that is produced inside the cells) which will cause a subsequent increase in the SSC signal. Therefore, it is beneficial to know for certain the cause of an increased SSC signal as this change could be due to the apoptosis process or nanoparticle uptake. A quick way to distinguish between these two causes is to reference the change or lack thereof in the FSC, as many studies report no change of FSC when NPs are internalized, 12,33 including this work. Another way is to add a cell apoptosis analysis to identify the presence of an apoptotic process.

CONCLUSION

By increasing the incident laser wavelength, the scattering signal of cells with different AuNPs (AuNSs and AuNRs) concentrations can be much better differentiated. This simple method with its ability to sort cells based on specific nanoparticle content will be very useful in detecting cellular gold nanoparticles. The greatest advantage of using flow cytometry is its ability for analyzing large numbers of live cells which can be effective in subsequent studies, such as proteomics, gene sequencing, and Western blot.

ASSOCIATED CONTENT

Supporting Information

The Supporting Information is available free of charge on the ACS Publications website at DOI: 10.1021/acs.analchem.9b02248.

Characterization of gold nanoparticles, cell viability assay, forward and side scattering information (PDF)

AUTHOR INFORMATION

Corresponding Authors

*E-mail: mali43@mit.edu or moustafa.r.k.ali@gmail.com (M.R.K.A.).

*E-mail: melsayed@gatech.edu (M.A.E.-S.).

ORCID ®

Yue Wu: 0000-0001-7680-9285

Moustafa R. K. Ali: 0000-0002-2027-1006 Mostafa A. El-Sayed: 0000-0002-7674-8424

Present Address

*Moustafa R. K. Ali: Department of Biological Engineering, Massachusetts Institute of Technology, Cambridge, Massachsetts 02139, United States

Author Contributions

The manuscript was written through contributions of all authors. All authors have given approval to the final version of the manuscript.

Notes

The authors declare no competing financial interest.

ACKNOWLEDGMENTS

We thank Mr. Ziyan Wu, undergraduate research assistant in El-Sayed's lab, for his help in performing experiments for gold nanosphere synthesis and flow cytometry analysis. We also thank Ms. Sommer Durham for her technical support of using the flow cytometry facility. Y.W., M.R.K.A. and M.A.E.-S. acknowledge the National Science Foundation (Grant 3306JR9) for its support of this work. K.D. and Y.W. acknowledge funding support from the Petit Undergraduate Research Scholars Program.

REFERENCES

- (1) Eustis, S.; el-Sayed, M. A. Chem. Soc. Rev. 2006, 35 (3), 209-
- (2) Murphy, C. J.; Gole, A. M.; Stone, J. W.; Sisco, P. N.; Alkilany, A. M.; Goldsmith, E. C.; Baxter, S. C. Acc. Chem. Res. 2008, 41 (12), 1721–1730.
- (3) Bardhan, R.; Lal, S.; Joshi, A.; Halas, N. J. Acc. Chem. Res. 2011, 44 (10), 936-946.
- (4) Cho, E. C.; Glaus, C.; Chen, J.; Welch, M. J.; Xia, Y. Trends Mol. Med. 2010, 16 (12), 561-573.
- (5) Huang, X.; El-Sayed, M. A. J. Adv. Res. 2010, 1 (1), 13-28.
- (6) Jain, P. K.; Lee, K. S.; El-Sayed, I. H.; El-Sayed, M. A. J. Phys. Chem. B 2006, 110 (14), 7238-7248.
- (7) Oyelere, A. K.; Chen, P. C.; Huang, X.; El-Sayed, I. H.; El-Sayed, M. A. *Bioconjugate Chem.* 2007, 18 (5), 1490–1497.
- (8) Dam, D.; Lee, J.; Sisco, P.; Co, D.; Zhang, M.; Wasielewski, M.; Odom, T. ACS Nano 2012, 6 (4), 3318-3326.
- (9) Cho, E.; Zhang, Q.; Xia, Y. Nat. Nanotechnol. 2011, 6 (6), 385-391.
- (10) Vanhecke, D.; Rodriguez-Lorenzo, L.; Clift, M. J.; Blank, F.; Petri-Fink, A.; Rothen-Rutishauser, B. *Nanomedicine* 2014, 9 (12), 1885–1900.
- (11) Rosman, C.; Pierrat, S.; Henkel, A.; Tarantola, M.; Schneider, D.; Sunnick, E.; Janshoff, A.; Sönnichsen, C. Small 2012, 8 (23), 3683–3690.
- (12) Park, J.; Ha, M. K.; Yang, N.; Yoon, T. H. Anal. Chem. 2017, 89 (4), 2449-2456.
- (13) Liu, M.; Li, Q.; Liang, L.; Li, J.; Wang, K.; Li, J.; Lv, M.; Chen, N.; Song, H.; Lee, J.; Shi, J.; Wang, L.; Lal, R.; Fan, C. Nat. Commun. 2017, 8, 15646.
- (14) Jacques, S. Phys. Med. Biol. 2013, 58, R37-R61.
- (15) Nikoobakht, B.; El-Sayed, M. Chem. Mater. 2003, 15 (10), 1957-1962.
- (16) Liu, X.; Atwater, M.; Wang, J.; Huo, Q. Colloids Surf., B 2007, 58 (1), 3-7.
- (17) Orendorff, C. J.; Murphy, C. J. J. Phys. Chem. B 2006, 110 (9), 3990–3994.
- (18) Ali, M. R.; Snyder, B.; El-Sayed, M. A. Langmuir 2012, 28 (25), 9807-9815.
- (19) Shukla, R.; Bansal, V.; Chaudhary, M.; Basu, A.; Bhonde, R. R.; Sastry, M. Langmuir 2005, 21 (23), 10644-10654.
- (20) Alkilany, A. M.; Thompson, L. B.; Boulos, S. P.; Sisco, P. N.; Murphy, C. J. Adv. Drug Delivery Rev. 2012, 64 (2), 190–199.
- (21) Prencipe, G.; Tabakman, S. M.; Welsher, K.; Liu, Z.; Goodwin, A. P.; Zhang, L.; Henry, J.; Dai, H. J. J. Am. Chem. Soc. 2009, 131 (13), 4783–4787.
- (22) Ruoslahti, E.; Pierschbacher, M. D. Cell 1986, 44 (4), 517-518.
- (23) Desgrosellier, J. S.; Cheresh, D. A. Nat. Rev. Cancer 2010, 10 (1), 9-22.
- (24) Kalderon, D.; Roberts, B. L.; Richardson, W. D.; Smith, A. E. Cell 1984, 39 (3), 499-509.
- (25) Ali, M.; Wu, Y.; Ghosh, D.; Do, B.; Chen, K.; Dawson, M.; Fang, N.; Sulchek, T.; El-Sayed, M. ACS Nano 2017, 11 (4), 3716–3726.
- (26) Albanese, A.; Chan, W. ACS Nano 2011, 5 (7), 5478-5489.
- (27) Baram-Pinto, D.; Shukla, S.; Gedanken, A.; Sarid, R. Small 2010, 6, 1044-1050.
- (28) Huschka, R.; Barhoumi, A.; Liu, Q.; Roth, J. A.; Ji, L.; Halas, N. J. ACS Nano 2012, 6 (9), 7681-7691.

(29) Rehor, I.; Lee, K. L.; Chen, K.; Hajek, M.; Havlik, J.; Lokajova, J.; Masat, M.; Slegerova, J.; Shukla, S.; Heidari, H.; Bals, S.; Steinmetz, N. F.; Cigler, P. *Adv. Healthcare Mater.* 2015, 4 (3), 460–468.

- (30) Ali, M. R.; Ali, H. R.; Rankin, C. R.; El-Sayed, M. A. Biomaterials 2016, 102, 1-8.
- (31) Suzuki, H.; Toyooka, T.; Ibuki, Y. Environ. Sci. Technol. 2007, 41 (8), 3018-3024.
- (32) Zucker, R. M.; Daniel, K. M. Methods Mol. Biol. 2012, 906, 497-509.
- (33) Ibuki, Y.; Toyooka, T. Methods Mol. Biol. 2012, 926, 157-166.
- (34) Armbruster, D. A.; Pry, T. Clin. Biochem. Rev. 2008, 29 (Suppl1), S49-S52.
- (35) Zucker, R. M.; Daniel, K. M.; Massaro, E. J.; Karafas, S. J.; Degn, L. L.; Boyes, W. K. *Cytometry, Part A* 2013, 83 (10), 962–972.
- (36) Greulich, C.; Diendorf, J.; Simon, T.; Eggeler, G.; Epple, M.; Köller, M. Acta Biomater. 2011, 7, 347-354.
- (37) Toduka, Y.; Toyooka, T.; Ibuki, Y. Environ. Sci. Technol. 2012, 46 (14), 7629–7636.
- (38) Friedrich, R. P.; Janko, C.; Poettler, M.; Tripal, P.; Zaloga, J.; Cicha, I.; Dürr, S.; Nowak, J.; Odenbach, S.; Slabu, I.; Liebl, M.; Trahms, L.; Stapf, M.; Hilger, I.; Lyer, S.; Alexiou, C. *Int. J. Nanomed.* 2015, 10, 4185–4201.
- (39) Aioub, M.; Kang, B.; Mackey, M. A.; El-Sayed, M. A. J. Phys. Chem. Lett. 2014, 5 (15), 2555-2561.
- (40) Panikkanvalappil, S. R.; Hooshmand, N.; El-Sayed, M. A. Bioconjugate Chem. 2017, 28 (9), 2452-2460.